

N71-75338

## 4. CONFIGURATIONS CONSIDERATIONS

By Roger W. Luidens, John H. Disher, Murray Dryer,  
and Thaine W. Reynolds

This paper provides a bridge between the preceding discussions of engines and the following discussion of the range capabilities of airplanes. Hence, consideration is given to the aerodynamics of configurations in terms of their lift-drag ratios and the effect of the propulsion system on the configuration. Finally, some factors affecting airframe structural weight are discussed.

The range equation is as follows:

$$\mathcal{R} = IV \frac{L/D}{1 - \left(\frac{V}{V_S}\right)^2} \ln \frac{1}{\frac{W_e}{W_G} + \frac{W_s}{W_G} + \frac{W_p}{W_G}} \quad (1)$$

where

I specific impulse

V velocity

$V_S$  satellite velocity

$W_e$  engine weight

$W_s$  structural weight

$W_p$  payload weight

$W_G$  gross weight

At a specified altitude,

$$\frac{W_e}{W_G} \approx \frac{1}{L/D}$$

The lift-drag ratio  $L/D$  is important because it affects the range directly and it also affects the range through the engine weight  $W_e$ . It affects engine weight in such a way that increasing lift-drag ratios

decrease engine weight. The airplane structural weight  $W_s$  enters the range equation in the same manner as the engine weight. Decreasing engine and structure weights increase range.

Consideration will first be given to configuration  $L/D$ . The drag of an airplane may be broken down in several ways. One way is (1) friction drag, (2) pressure drag at zero lift, and (3) drag due to lift. Another classification might be (1) fuselage drag, (2) wing drag, and (3) engine drag. Unfortunately, it is not possible to consider these items as isolated topics. Therefore, although each of the items mentioned is discussed, it is always discussed in relation to the over-all problem of achieving long range.

The lift-drag ratios considered today are much higher than those considered several years ago. This fact is related in a large part to a very fundamental effect - airplane size.

Two schematic airplanes, one with a gross weight of 20,000 pounds and the other with a gross weight of 500,000 pounds, are shown in figure 1. The equation at the top of the figure is for the zero-lift drag coefficient of the airplane based on wing area  $C_{D,0}$ . It is equal to the zero-lift drag coefficient of the wing  $C_{D,0,W}$  plus the zero-lift drag coefficient of the body based on the body area  $C_{D,0,b}$  times the ratio of body area to wing area  $A_b/S_w$ . The latter ratio is necessary to make the equation consistent. The so-called "square-cube law" states that, if the linear dimensions of a body are increased, the areas will increase as the square of the linear dimension and the volume will increase as the cube. For example, if the size of the small airplane is doubled, the wing area will be four times as big as the original area, and the volume will be eight times larger than the original volume. If it is assumed that the two airplanes shown in the figure have the same wing loading, scaling up the small configuration will result in more volume in the body than needed. In addition, there is relatively more usable volume in the wing of a large airplane. This means that the ratio of body area to wing area can be reduced; and therefore the last term in the drag equation is reduced.

The airplane size also reduces the coefficients in the drag equation. Figure 2 is the familiar plot of the variation of mean skin-friction coefficient with free-stream Reynolds number. This particular curve is for a turbulent boundary layer at Mach 4. The coefficient that might be expected for a 20,000-pound airplane is about 0.0013, and for a 500,000-pound airplane is about 0.0010. The larger airplane has a lower friction coefficient.

These two effects, reduction of skin-friction coefficient and reduced body drag coefficient as a result of increased size, have been combined

in a calculation of maximum lift-drag ratio as a function of gross weight (on a log scale) in figure 3. The 20,000-pound airplane has a maximum  $L/D$  of about 6.0, whereas the larger airplane has a value of about 8.5. By increasing the gross weight still further, a point is reached where all the necessary volume is readily available in the wing, and an even higher  $L/D$  results.

The flight Mach numbers of interest have also increased over the last several years. Figure 4 is a plot of friction coefficient against Reynolds number for flight Mach numbers of 2, 4, and 7. Increasing  $M_0$  also tends to decrease the friction coefficient. However, there is another factor that influences  $(L/D)_{\max}$ . One form of the equation for maximum  $L/D$  is as follows:

$$\left(\frac{L}{D}\right)_{\max} = \frac{1}{2} \sqrt{\frac{dC_L/d\alpha}{C_{D,0}}} \quad (2)$$

Besides the drag  $C_{D,0}$ , the lift-curve slope  $dC_L/d\alpha$  also enters into the determination of  $(L/D)_{\max}$ . In general, the lift-curve slope decreases more rapidly with increasing Mach number than the drag decreases. The net result is that  $(L/D)_{\max}$  generally decreases somewhat with increasing  $M_0$ . This effect will be evident in several of the later figures.

The drag of an airplane is also affected by the nature of the boundary layer, whether it is turbulent or laminar. Figure 5, which shows friction coefficients for laminar and turbulent boundary layers, indicates that, if the boundary layer is laminar, the skin-friction coefficient is considerably lower than if the boundary layer is turbulent. This decrease in the friction coefficient may be reflected in a considerable increase in the lift-drag ratio. Since this is the case, one should look into the probability of obtaining laminar flow at the flight conditions being considered.

Figure 6 shows a band of Reynolds numbers for a 60-foot-long surface calculated for the particular altitude and Mach number variations shown in the upper right corner of the figure. The points plotted are experimental values and are some of the highest Reynolds numbers at which laminar flow has been observed in free flight. The arrows on the points indicate that the flow, in fact, was laminar at the last measuring station on the body, and that transition to turbulent flow would have occurred at higher values of Reynolds numbers than those indicated. The fact that the range of Reynolds numbers of interest may be below values at which laminar flow has been observed would indicate that a good chance of obtaining laminar flow exists in these cases.

However, Reynolds number is not the only criterion for determining the transition from laminar to turbulent flow. The effects of some of

the additional factors that influence boundary-layer transition are shown in figures 7 and 8. The Reynolds number of figures 6, 7, and 8 is based on length from the stagnation point of the body and on free-stream conditions. Figure 7 shows calculated transition characteristics for blunt-nosed bodies at Mach 5 (based on data of refs. 1 to 4 and theory of ref. 5), and figure 8 presents flight and wind-tunnel transition data for sharp-tipped bodies at Mach numbers of 3 to 5 (refs. 1 and 4). Both figures show the favorable effect of low wall to stream temperature ratios on increased transition Reynolds number. The unfavorable effect of surface roughness is shown by the decrease in transition Reynolds number at a given temperature ratio. Approximate values of average surface roughness for the "smooth" and "rough" data were 2 to 16 microinches and 200 microinches, respectively. The favorable effect of tip bluntness on increased transition Reynolds number is apparent. This effect is due to the lowering of Reynolds number and the increase of static temperature at the edge of the boundary layer, as discussed in reference 5. The size of the blunt tip required to achieve the favorable effect varies with model length and with stream conditions. When the nose of the body is blunted in order to enhance the chances for laminar flow, the added pressure drag due to bluntness must of course be weighed against the decreased friction drag. In addition, if the tip bluntness becomes too large, transition may occur on the tip itself; thus, the amount of tip bluntness must be carefully considered.

To illustrate the place of typical flight conditions in these curves, a flight condition for Mach 5 at 100,000 feet altitude with a 60-foot-long body at radiation equilibrium wall temperature is shown on the coordinates of figures 7 and 8. If the body is blunt tipped the flight condition lies in the laminar region for smooth bodies, but when roughness is considered it appears likely that turbulent flow would exist over much of the body. With a sharp-tipped body, the flight condition would be in the turbulent region even with smooth surfaces. In order for the flight condition to lie in the laminar region for the sharp-tipped body, the wall would have to be cooled well below the equilibrium temperature.

Additional adverse effects on laminar boundary layers are caused by control-surface-body or wing-body junctures and protuberances such as pilot canopies. The transition data shown are for bodies alone. The limited amount of data available indicate that early transition to turbulent flow is likely to occur aft of body-wing junctures.

The amount of wing friction drag can be large compared with the total drag for configurations with large wings. Therefore the amount of laminar flow that might be expected on a wing must be considered. Some experimental data in figure 9 show the effect of wing sweep on transition. The sketch defines the distance  $X_T$  where transition occurs perpendicular to the wing leading edge. The distance, shown as a fraction of the distance for a zero-sweptback wing, is plotted as a function of the angle of

sweep. The Mach 4 experimental data (ref. 6) agree quite well with the cosine-cubed of the sweepback angle. If highly swept wings ( $65^\circ$  to  $75^\circ$ ) are to be used, it appears very unlikely that significant runs of laminar flow can be expected.

The boundary-layer discussion may be summarized as follows. On some highly polished, slightly blunted research models, laminar flow has been observed to very high Reynolds numbers. But on a practical airplane that flies at angle of attack, has a pilot canopy and canard surfaces on the fuselage forebody, and has skin joints, or on a wing that is highly swept, long laminar runs seem improbable.

It is appropriate to discuss another point here. A hot, highly stressed structure such as the wing will probably develop a surface waviness. This waviness will generate a pressure drag that is not usually included in the form drag and is often charged to the surface drag. With this waviness condition, the drag chargeable to the surface can be larger than that calculated by assuming all-turbulent skin friction. (The Missions Studies paper (5) assumes all-turbulent boundary layer in calculations.)

Consider next the pressure drag, in particular as it relates to fuselage design. There are two philosophies about fuselage design. One is that the fuselage should house a given volume at the minimum cost in drag. If this is the point of view, the analysis shown on figure 10 may be made. The drag per fuselage volume is plotted against fuselage fineness ratio  $l/d$ . Increasing the fineness reduces the pressure drag but increases the friction drag because the wetted area increases. (A sphere,  $l/d = 1.0$ , has a minimum wetted area for given volume.) The sum of the friction and pressure drag reaches a minimum at  $l/d$  of about 25 in this example. From an engineering point of view, this minimum drag is essentially reached at  $l/d$  of 18 or 20. The airplane models with circular fuselages have finenesses of 18 and 20.

A second approach to fuselage design is to find the fuselage shape that will give the best airplane  $L/D$ . An example of the results from such an approach is shown in figure 11. In this example the fuselage volume and flight altitude are held constant. The lift-drag ratio is plotted against the width to height ratio of the fuselage and against the length over the equivalent diameter of fuselage. The upper curve is the  $L/D$  of the wing alone, which is 8.3. The point at  $w/h = 1$  is for a circular nonlifting fuselage, and at this point  $L/D$  of the wing-body combination is 6.0. Carrying lift on the fuselage and widening it to make it a better lifting shape increases the  $L/D$  of the wing-body combination to a value approaching 7.0. For  $w/h = 4.0$ , the effect of equivalent fineness is shown on the right side of figure 11. The best  $l/d$ , about 16, is somewhat less than the  $l/d$  of about 25 for the previous analysis.

There are other ways of generating lift from the fuselage. The Ames configuration uses a half cone under an arrow wing. Antonio Ferri discusses still another design approach that might be applied to a fuselage in the Journal of the Aeronautical Sciences for November 1957.

The choice of design approach is related in part to the fuel-tankage problem, as will be discussed shortly. The idea here is that, for a configuration design to have the highest aerodynamic efficiency, all the components of the airplane must do their share of the work. The fuselage generates a pressure and friction drag; it should also generate its share of the lift.

The next drag term to be examined is the drag due to lift, illustrated in figure 12. There are ways to minimize this drag term. In supersonic flow with a conventional supersonic airfoil at angle of attack (illustrated as a flat plate in the upper left corner of fig. 12), it is evident that the resultant force vector for the airfoil lies perpendicular to the surface and that a drag direction force  $D_i$  equal to the resultant force  $R$  times the sine of the angle of attack  $\alpha$  exists. In subsonic flow, illustrated at the lower left of the figure, camber and a rounded leading edge on an airfoil make it possible to take advantage of leading-edge suction and thus bring the resultant force vector, in the idealized two-dimensional case, normal to the free stream and eliminate the drag term. A concept that would apply this subsonic principle to supersonic flow is illustrated at the lower right. Here a subsonic airfoil is swept back so far that the Mach number normal to the leading edge of the airfoil is subsonic. In this situation, leading-edge suction can be utilized to bring the resultant force vector nearly perpendicular to the free stream.

Figure 13 shows calculated lift-drag ratios for this type of wing, which has been called the oblique wing. The calculated values are based on experimental section data for the 64A-506 subsonic airfoil section. For comparison, calculated lift-drag ratios for a conventional supersonic airfoil of  $2\frac{1}{2}$ -percent thickness are shown by the dashed line. At a Mach number of 2, the oblique wing shows over twice the maximum lift-drag ratio of the conventional wing. Of course, the calculations shown apply to the two-dimensional case. When finite aspect ratios are considered, the values will decrease. Recent experiments with an oblique wing in the Lewis 1- by 1-foot Mach 3 wind tunnel have yielded encouraging results.

It should be remarked that the oblique-wing concept is about 12 years old; and, although it appears to be very interesting, it evidently has not been thoroughly exploited. Section data for airfoils up to 10 or 12 percent thick indicate that they may also yield good L/D. For very large airplanes, using wings of such thickness, it is possible to conceive a flying-wing airplane where all the required volume is in wing. Such a flying-wing configuration would be expected to have a very high L/D. This is certainly an interesting possibility.

**CONFIDENTIAL**

This concludes the discussion of wing and fuselage drag. One topic remains that can have a marked effect on the airplane configuration and its lift-drag ratio; that is, the effect of the propulsion system - fuel type and engine location.

Two fuels have been prominent in the discussions of the preceding papers - JP fuel and hydrogen. One of the significant differences in these fuels is their density. JP fuel has a density of 47 pounds per cubic foot; hydrogen, 4.4 pounds per cubic foot. The effect of this density difference on the airplane configuration is illustrated by the two models in figure 14. The JP airplane has a gross weight of 500,000 pounds. The hydrogen airplane actually has a lower gross weight, 300,000 pounds, but is almost twice as long. In addition, the hydrogen airplane has a larger ratio of fuselage to wing area. This has an adverse effect on the L/D, as previously discussed.

The other propulsion-system factor of interest is the engine installation. Of course, the objective is to find a way to install the engine to the mutual benefit of both the engine and the airframe.

Consider first the question of engine inlet location. There are a number of reasons why it is desirable to locate the engine inlet under a wing or fuselage to take advantage of the compression field there. Some of these reasons are illustrated in figure 15, which shows two examples of locating the engine inlet under a wing. First, the size of the inlet is reduced from what it would be if located in the free stream. At Mach 4, the inlet area is reduced about 30 percent. At Mach 7, the area reduction is about 50 percent. This reduced inlet area for the turbojet engine ( $M = 4.0$ ) would ease the matching problem at lower speeds. Another reason is that the Mach number ahead of the inlet is reduced below the free-stream value, and this would tend to increase the pressure recovery of the inlet. Also, shielding the inlet in this way would make the performance of the inlet insensitive to variations in angle of attack.

This inlet area reduction has an effect on the over-all engine proportions, as illustrated in figure 16. Here the engine frontal area is shown in a two-dimensional fashion for a Mach 4 turbojet installation. Assuming that an exit static-pressure ratio of 1.7 is acceptable as a compromise between the jet thrust and cowl pressure drag for a nacelle installation, the top sketch illustrates the frontal area when the inlet is located in the free stream. When the inlet is located under the wing or body, the frontal area will be increased, as shown by the middle sketch. If complete expansion is desired, the frontal area increases still further, as shown by the bottom sketch. This increased frontal area can be an advantage or a disadvantage, as illustrated by the configurations in figures 17 and 18. Figure 17 shows the engines mounted in nacelles beneath the wing. The pressure drag on the engines will be higher than it would be if the nacelles were in the free stream, because the pressures and the

frontal areas are larger. The configuration of figure 18 has the inlet beneath the body. Complete expansion is utilized in the nozzle. The pressure drag on the engine frontal area has been avoided because the engine frontal area is hidden behind the main body frontal area. In addition, the fuselage afterbody pressure drag, which is unavoidable on the previous configuration, is decreased or eliminated.

Another way the engine can be used to improve the performance of the configuration is to take lift from the exhaust jet. This can be done by canting the jet downward. An example of this is given in figure 19 for a Mach 4.0 turbojet. Relative range is plotted as a function of the angle of jet cant below the flight direction  $\theta$ . Airplane performance is often calculated as if the jet is aligned in the flight direction ( $\theta = 0$ ). By canting the jet to the optimum angle, which is about twice the wing angle of attack, a 4-percent gain in range is available. The size of this range gain depends for one thing on the airplane  $L/D$ . For lower values of  $L/D$ , the range gain would be larger. With respect to maintaining faired external lines on the over-all airplane and avoiding unbalance moments, it often is inconvenient to cant the exhaust jet more or less than the wing angle of attack. A range gain resulting from canting the exhaust at the angle of the wing, in this case 3 percent, exists in most airplane designs.

Another consideration associated with engine inlet location is directional stability. Figure 20(a) illustrates an airplane with a circular fuselage cross section and with the engine inlet located at the front. This is a poor location with respect to stability, since, if the airplane is yawed slightly, the force required to turn the incoming air tends to increase the yaw angle. The unstable condition is indicated in figure 20(a) by the "inlet" curve. The body is also directionally unstable; this condition of instability for the inlet-body combination is also indicated in figure 20(a).

The area of a tail required to make this airplane neutrally stable at Mach 7 can be calculated. This configuration would be more stable at lower Mach numbers, indicating that the condition that designs the tail is the high Mach number. The addition of such a tail surface might reduce the  $L/D$  of the configuration from 7.5 to around 7.1.

Figure 20(b) shows a configuration with the engine inlet located to the rear of the airplane center of gravity and with a flattened fuselage. This fuselage has the same volume as the circular one of figure 20(a). The advantage of this flattening to obtain lift from the fuselage was mentioned earlier. This shape also reduces the cross section of the body normal to the yaw direction, and so directional instability of the body is reduced. Since the engine inlet is behind the center of gravity, the turning force tends to restore the airplane to the flight direction. This combination, then, can be made directionally stable without the addition of any tail surface. A tail surface might be required, however, for proper control and dynamic characteristics.

In figure 21 some experimental maximum lift-drag ratios are plotted as a function of free-stream Mach number for several airplane concepts. One scheme is the Ames configuration sketched in figure 22. This model, tested in the Ames 10- by 14-inch tunnel, incorporates half of a hypersonic body of revolution mounted beneath an arrow wing. The pressure field of the body therefore produces lifting pressures on the underside of the wing. The data shown as solid symbols in figure 21 were obtained at Reynolds numbers of  $5.2 \times 10^6$  to  $1 \times 10^6$  based on the model length of 7 inches. The Reynolds number decreased with increasing Mach number. The maximum  $L/D$  varies from a little over 7 at Mach 3 and 4 to about 5 at Mach 6.2.

Another configuration investigated recently in the Lewis 10- by 10-foot tunnel is the flat-bottom design shown in figure 23. This fuselage has a semielliptical cross section and a canopy that was necessary to accommodate the sting and strain-gage balance assembly. The wing is swept back at about  $74^\circ$  and is hexagonal in cross section. Thickness of  $1/4$  inch gives a thickness-chord ratio at the mean aerodynamic chord of less than 1 percent. The wing is made of aluminum and is extremely flexible, but no flutter was encountered. The data were obtained at Reynolds numbers of  $6.6 \times 10^6$ ,  $20 \times 10^6$ , and  $29 \times 10^6$ , based on the body length of 13.2 feet, and at Mach numbers of 3.0 and 3.5. At Mach 3.0 the maximum  $L/D$  of 6.9 at  $6.6 \times 10^6$  Reynolds number was increased to 9.3 at  $Re_\ell$  of  $20 \times 10^6$ . This is due in large part to the effect of Reynolds number on the friction coefficient, which was discussed earlier.

Data for a third configuration are also shown. These data were obtained for what might be called a conventional wing-body configuration (fig. 24). The data shown are for the configuration without the engines. At the high Reynolds number of  $29 \times 10^6$  the data fall from about 6 at Mach 2 to about 5.5 at Mach 3.5. It should be emphasized that all these data are for configurations without engine installations or tail surfaces.

Consider again the range equation (eq. (1)). Several factors affect the airplane structural weight  $W_s/W_G$ . The discussion of inlets and outlets in paper 2 pointed out the large effect of the temperature environment on the engine design. The temperature environment around the airplane structure can also have an important effect on the airframe structural design and weight. Another item that can make a substantial contribution to structural weight is the fuel tank. This is particularly true for hydrogen. And, of course, this tank problem is aggravated by its temperature environment.

Shown in figure 25 are radiation equilibrium surface temperatures at selected locations on a typical airframe. These temperatures are shown as a function of Mach number for the Mach number and altitude schedule shown on the figure. The calculations are for turbulent flow with 0.8 emissivity. The lower curves show wing upper- and lower-surface

temperatures at  $5^\circ$  angle of attack. At Mach 9, the wall temperature is less than  $1700^\circ \text{R}$ . If necessary, the entire wing structure could be built to withstand this temperature. At the wing leading edge, the temperature exceeds  $2400^\circ \text{R}$  at Mach numbers above 7, and leading-edge cooling would be required. The wing temperatures shown would also apply approximately to the upper and lower surfaces of the fuselage and to the fuselage stagnation region.

The amount of cooling required for the airframe is shown in figure 26. The airframe configurations are those chosen for the range calculations in the Mission Studies paper (5). Although it should be possible to build a wing to withstand equilibrium temperature, it may be more efficient structurally to have a cool internal structure. For that reason, the cooling requirements have been based on  $600^\circ \text{F}$  internal wing temperature. The leading-edge requirement has arbitrarily been taken as  $1600^\circ \text{F}$ , and the fuselage interior other than fuel tankage areas as  $170^\circ \text{F}$ . The use of 1 inch of insulation is assumed, where required. The cooling requirement is expressed in percent of available cooling capacity for hydrogen fuel. At Mach numbers of 4 to 5 only a slight amount of cooling is required. At Mach 7, about 6 percent of that available is needed, and at Mach 9 this has risen to 10 percent. It was shown in paper 2 that about 50 percent of the available fuel cooling capacity is required for the engine alone. Thus, the total required cooling capacity for airframe and engines would be approximately 60 percent of the total available cooling capacity of the fuel at Mach 9.0. The requirement is conservative in the sense that a cooled wing structure is provided for.

With regard to fuel storage in the airplane, this discussion merely presents some considerations indicating the order of magnitude of the tank weights and fuel vaporization rates with hydrogen. Consider, first, just the weight of the tank shell required to house a given quantity of fuel. As shown on figure 27, the weight of tank per unit weight of fuel will be proportional to the surface-volume ratio of the tank and to the thickness and density of the construction materials, and inversely proportional to the fuel density. If one considers making this tank from a minimum-gage-thickness material (in this case 0.015-inch stainless steel), the weight of the tank shell alone for hydrogen is shown by the middle curve of figure 27 as a function of tank diameter. Since the surface-volume ratio is inversely proportional to the diameter, the increase of weight at small diameters represents one penalty connected with configurations that require a small tank diameter. Tanks of the particular thickness shown would have the maximum operating pressures shown on the curve; that is, the yield limit would be reached at these pressures and any desired higher operating pressure would require proportionately heavier tanks.

Similarly, the weight of any insulation required would be governed in the same manner,  $\rho$  and  $t$  being the density and thickness of the

insulation. A curve of insulation weight for a 2-inch layer is also shown. The use of this insulation will be discussed shortly. The combined weight of a tank shell plus 2 inches of insulation, again for hydrogen, is shown by the top curve of figure 27. In the range of tank diameters that are involved in some of the configurations presented in the following paper (6 to 7 ft), minimum tank weights would be in the neighborhood of 15 percent of the fuel weight with present materials. The higher density of JP fuels, 10 times that of hydrogen, would give much smaller tank weights by these criteria.

The weight of insulation shown in figure 27 has been used in two different ways, as shown in figure 28. In one way, which is labeled "nonregenerative," the insulation is a simple barrier between the fuel tank and the fuselage. Heat flowing into the fuel tank all goes into latent heat and vaporizes fuel. The other way of using the same amount of insulation is called a "regenerative" system. This scheme essentially splits the insulation into two layers and permits vaporized gas to circulate between the layers. Using this principle, it is possible to take advantage of considerably more of the heat-sink capacity of the fuel than in the nonregenerative system, which absorbs only latent heat. In effect, in the regenerative system, heat that flows through the inner layer of insulation goes to the vaporizing fuel, while gas circulating between the layers intercepts and carries off a large portion of the heat flowing through the outer layer.

A comparison of the performance with these two methods is shown in figure 29 as a function of flight Mach number. The heat-transfer performance of the insulation at the higher Mach numbers is related to two different effects. One is the higher fuselage temperatures which lead to greater heat-transfer rates. The other is the higher fuel-flow rate. This higher fuel flow may be considered a counteracting effect, since the general concern is with the rate of fuel vaporization compared to the fuel-flow rate to the engines. In this illustration the higher fuel-flow rates at the higher Mach numbers more than counteracted the effect of the higher temperatures.

With the nonregenerative insulating scheme (top curve of fig. 29), vaporization rates of the order of 60 to 70 percent of the fuel-flow rate were calculated for a particular configuration over a range of conditions. With vaporization rates of this order of magnitude, pumping large quantities of vapor fuel would be necessary. This increased pumping would require either higher-pressure tanks (using tank pressure as the pumping means), which means heavier tanks, or vapor pumps, which also may be large and heavy.

Using the regenerative scheme, calculated vaporization rates were only 6 to 7 percent of the fuel-flow rate, or about one-tenth of that for the nonregenerative system (fig. 29). It would seem, then, that some such scheme as the regenerative one will be required to avoid the necessity for handling large quantities of vapor fuel.

To summarize the ideas discussed in this paper, several models incorporating as many of the favorable features as possible were built and are shown in figure 30. Figure 30(a) is a Mach 4.0 airplane of 500,000-pound gross weight using JP fuel. Because tank weight is not a problem with JP fuel, a flattened fuselage is used to develop fuselage lift. The forebody is shaped in plan form for low center-of-pressure shift from subsonic to supersonic speeds and is cambered in side view for self trim without a canard surface. The shape of the bottom of the fuselage results in a favorable pressure gradient. Since there is no canard surface, it is hoped that a long run of laminar boundary layer will exist. The inlet is located under the fuselage to take advantage of the compression existing there and to shield the inlet from angle-of-attack effects. It is located behind the center of gravity to contribute to the directional stability. The engine frontal area is hidden behind the fuselage, eliminating engine pressure drag and fuselage afterbody drag. The exhaust is at the wing angle of attack to develop some jet lift. The airplane probably does not require airframe structural cooling.

The airplane shown in figure 30(b) is designed for Mach 4.0 using hydrogen and has a gross weight of 300,000 pounds. Despite the lower gross weight, the hydrogen-fueled airplane is about twice as long. Because fuel tankage is a problem of prime importance for the hydrogen airplane, only a partially widened fuselage was used. A canard surface was chosen for trim and control. Most of the other features of the airplane are consistent with those previously described.

The final airplane shown in figure 30(c) is an adaptation of the oblique wing to an arrow-wing configuration. This type of configuration shows great analytical possibilities below  $M = 3$  or 4. More experimental evidence is needed, however.

The ideas about airplane configurations and their lift-drag ratios discussed in this paper have been incorporated in the range and mission calculations that are presented in paper 5.

#### REFERENCES

1. Rabb, Leonard, and Disher, John H.: Boundary-Layer Transition at High Reynolds Numbers as Obtained in Flight of a  $20^\circ$  Cone-Cylinder with Wall to Local Stream Temperature Ratios Near 1.0. NACA RM E55I15, 1955.
2. Disher, John H., and Rabb, Leonard: Observation of Laminar Flow on a Blunted  $15^\circ$  Cone-Cylinder in Free Flight at High Reynolds Numbers and Free-Stream Mach Numbers to 8.17. NACA RM E56G23, 1956.

SECRET

89

3. Rabb, Leonard, and Krasnican, Milan J.: Observation of Laminar Flow on an Air-Launched  $15^\circ$  Cone-Cylinder at Local Reynolds Numbers to  $50 \times 10^6$  at Peak Mach Number of 6.75. NACA RM E56L03, 1957.
4. Low, George M.: Boundary-Layer Transition at Supersonic Speeds. NACA RM E56E10, 1956.
5. Moeckel, W. E.: Some Effects of Bluntness on Boundary-Layer Transition and Heat Transfer at Supersonic Speeds. NACA Rep. 1312, 1957. (Supersedes NACA TN 3653.)
6. Dunning, Robert W., and Ulmann, Edward F.: Effects of Sweep and Angle of Attack on Boundary-Layer Transition on Wings at Mach Number 4.04. NACA TN 3473, 1955.

4793-I

SECRET

# LARGE AIRPLANES HAVE LESS FUSELAGE DRAG

$$C_{D,0} = C_{D,0,W} + C_{D,0,b} \left( \frac{A_b}{S_w} \right)$$

GROSS WT, LB

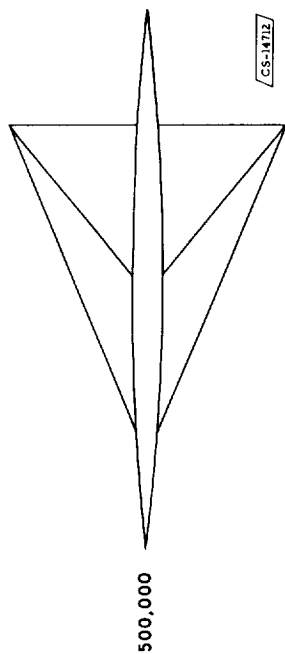


Figure 1

# LARGE AIRPLANES HAVE BETTER LIFT-DRAG RATIOS

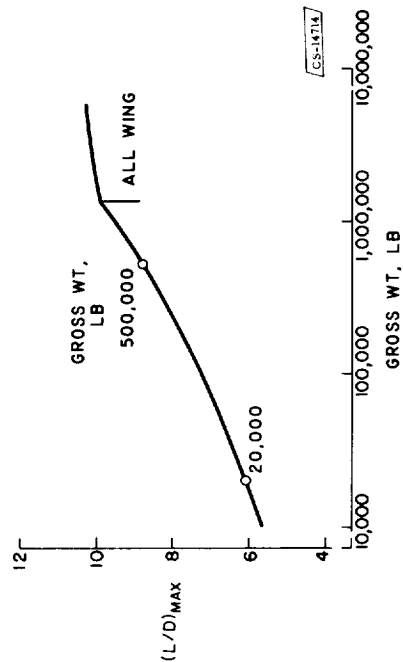


Figure 3

# LARGE AIRPLANES HAVE LESS FRICTION DRAG

$M_0 = 4$ , TURBULENT BOUNDARY LAYER

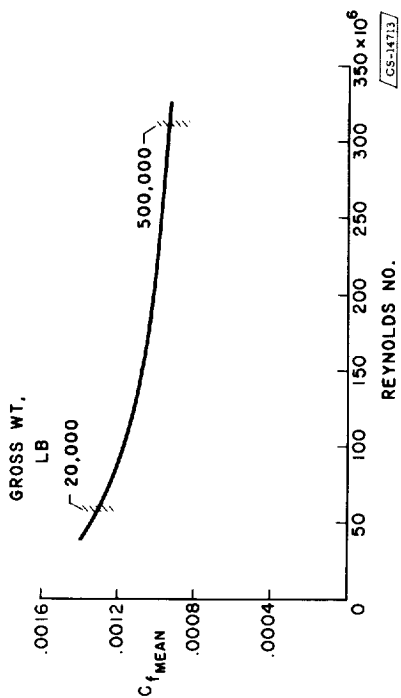


Figure 2

# INCREASED MACH NUMBER LOWERS FRICTION DRAG

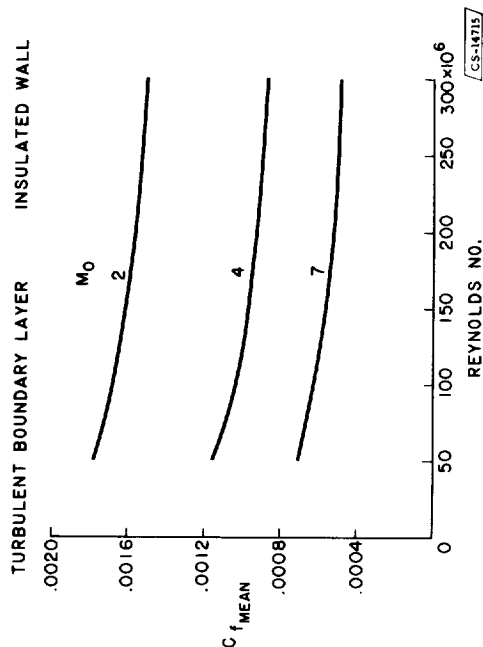


Figure 4

# LAMINAR AND TURBULENT FRICTION COEFFICIENTS

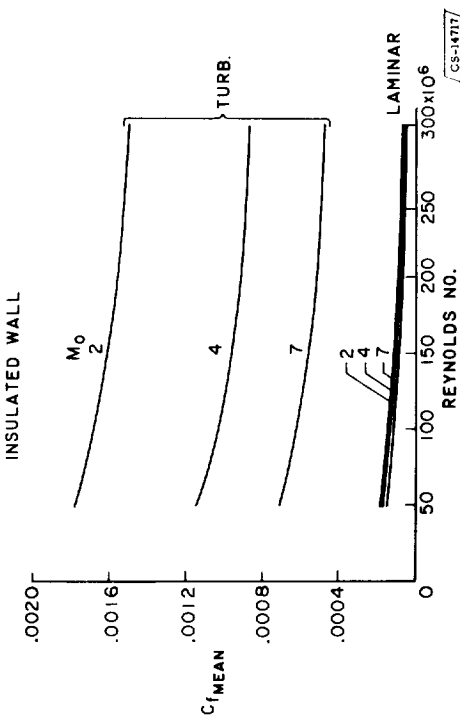


Figure 5

# TRANSITION FOR BLUNT-NOSED BODIES

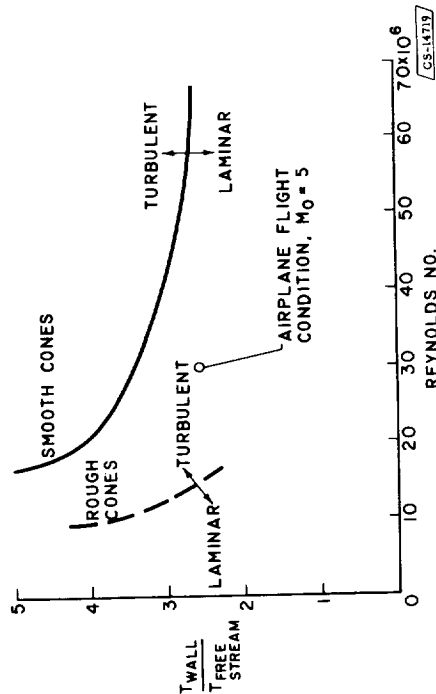


Figure 7

# AIRPLANE FLIGHT CONDITIONS

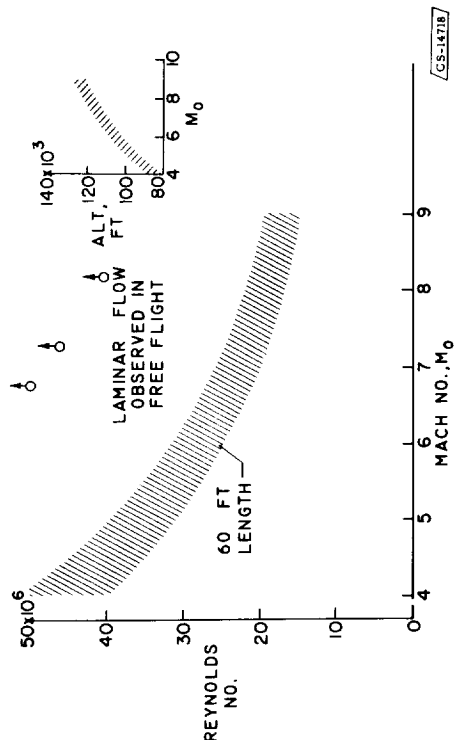


Figure 6

# TRANSITION FOR SHARP-NOSED BODIES

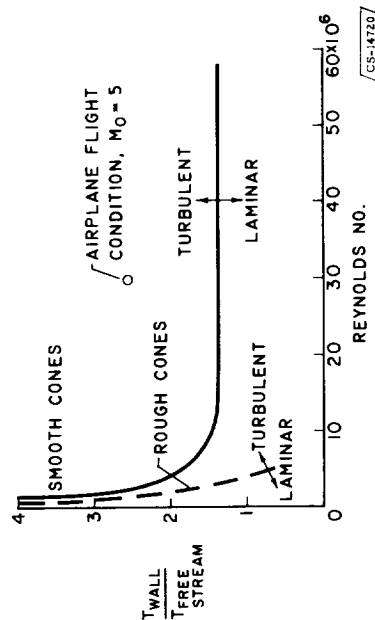


Figure 8

# WING SWEEP PROMOTES TRANSITION

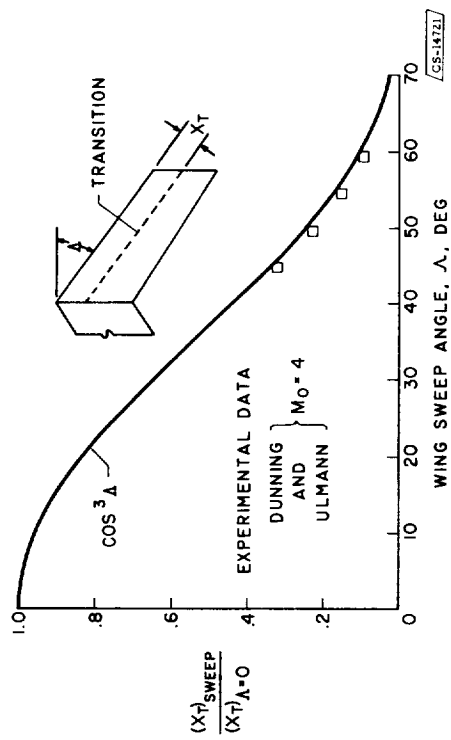


Figure 9

# FUSELAGE DRAG

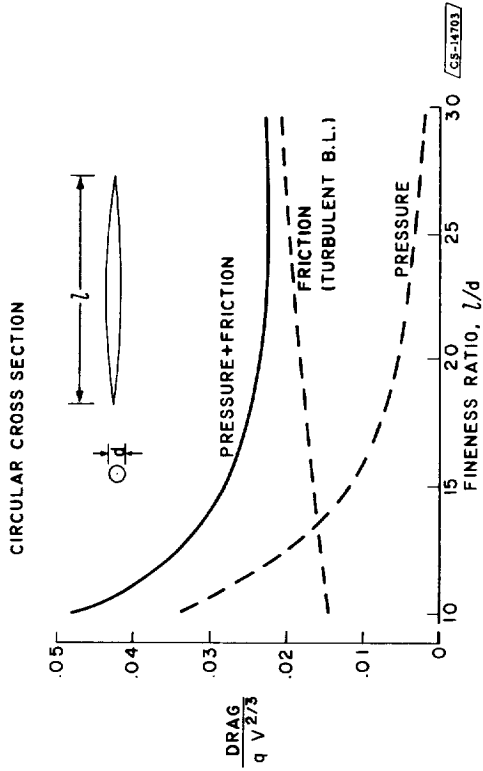


Figure 10

# LIFTING FUSELAGE CONSTANT VOLUME AND FLIGHT ALTITUDE

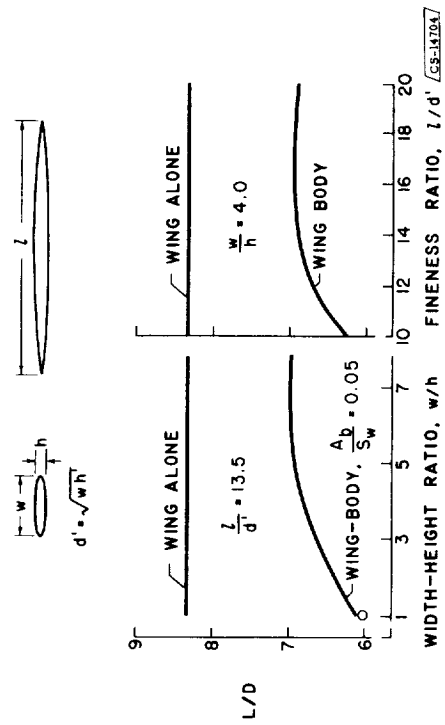


Figure 11

# SOME LIFTS DON'T DRAG

2-DIMENSIONAL

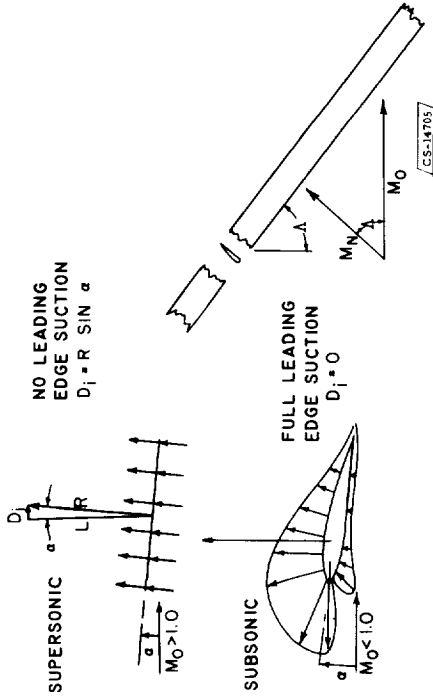


Figure 12

# EFFECT OF FUEL TYPE

HYDROGEN FUEL      JP FUEL  
GROSS WEIGHT, 300,000 LB      GROSS WEIGHT, 500,000 LB



Figure 14

# OBLIQUE WING LIFT-DRAG RATIO

2-DIMENSIONAL, TURBULENT BOUNDARY LAYER

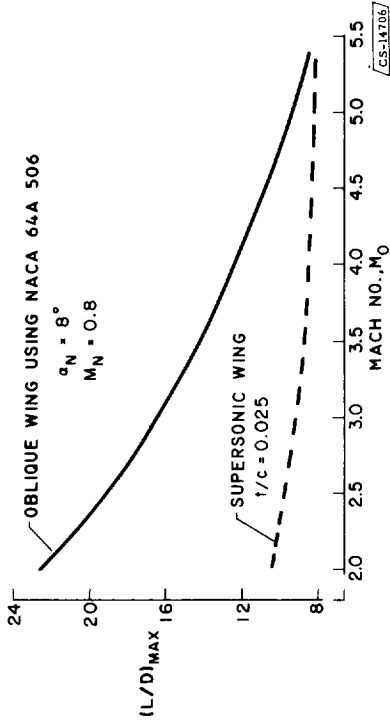


Figure 13

# INLET LOCATION

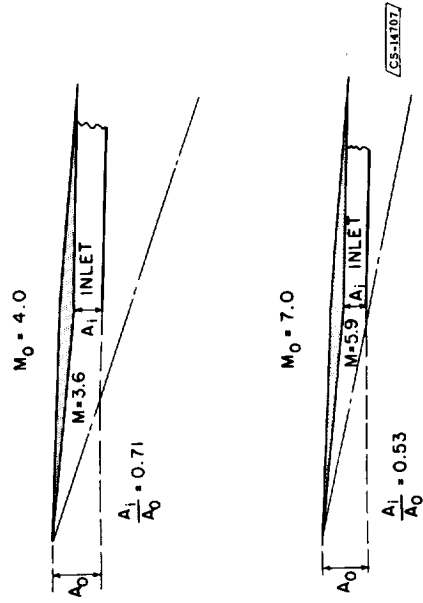


Figure 15

# ENGINE FRONTAL AREA TWO-DIMENSIONAL

ENGINE: MACH NO., 4 TURBOJET

INLET LOCATION:

IN THE  
FREE STREAM

$$\frac{P_{EXIT}}{P_0} = 1.7$$

UNDER THE  
WING OR BODY

$$\frac{P_{EXIT}}{P_0} = 1.7$$

UNDER THE  
WING OR BODY

$$\frac{P_{EXIT}}{P_0} = 1.0$$

CS-14708

Figure 16

# FUEL HYDROGEN

GROSS WT. 300,000 LB, ENGINES IN FUSELAGE

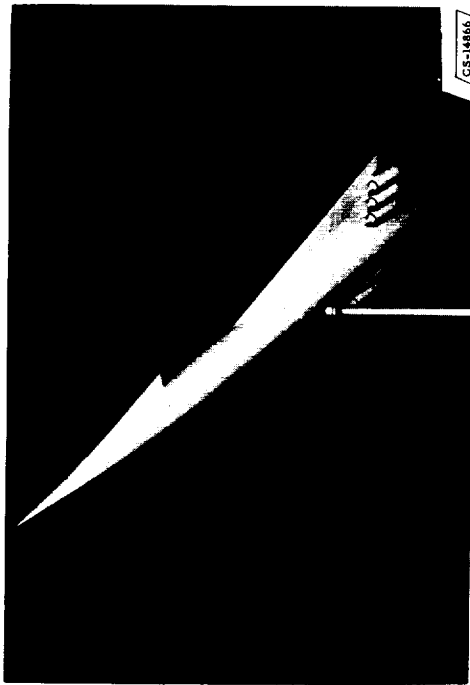


CS-14864

Figure 18

# FUEL HYDROGEN

GROSS WT. 300,000 LB, NACELLE ENGINES

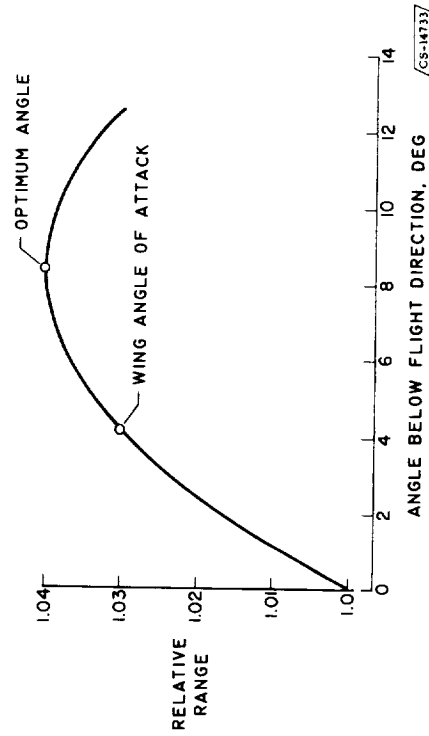


CS-14866

Figure 17

# JET CANT FOR LIFT

TURBOJET, M=4.0, (L/D)=70, Tcycle = 3000° R



CS-14737

Figure 19

# DIRECTIONAL STABILITY

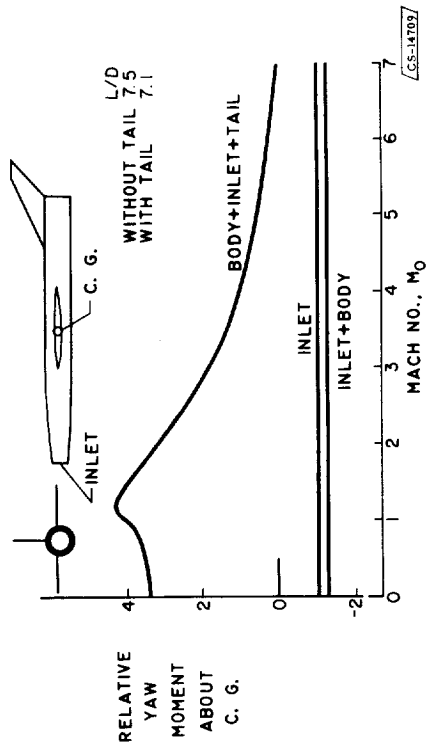


Figure 20(a)

# EXPERIMENTAL MAXIMUM LIFT-DRAG RATIOS

CONFIGURATION	FACILITY	Re <sub>L</sub>	SYMBOL
FLAT TOP	AMES (10" x 14")	5.2 x 10 <sup>6</sup> TO 1.0 x 10 <sup>6</sup>	•
FLAT BOTTOM	LEWIS (10' x 10')	29 x 10 <sup>6</sup> 20 x 10 <sup>6</sup> 66 x 10 <sup>6</sup>	◻ ◻ ◻
CONVENTIONAL WING-BODY	LEWIS (10' x 10')	29 x 10 <sup>6</sup>	Δ

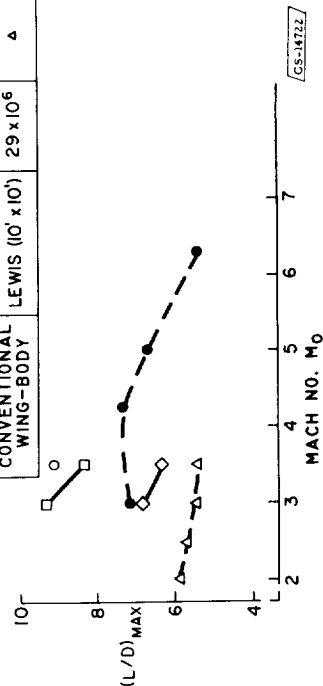


Figure 21

# DIRECTIONAL STABILITY

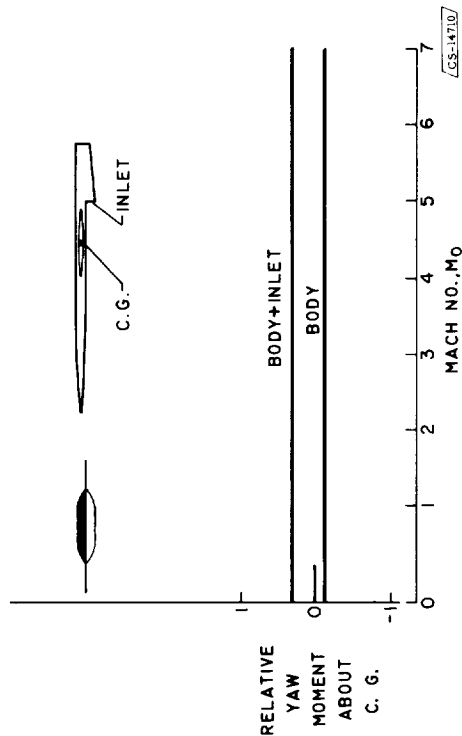


Figure 20(b)

# FLAT TOP CONFIGURATION (AMES)

10" x 14" SWT

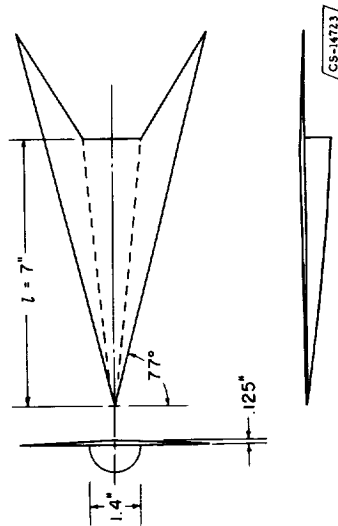


Figure 22

FLAT BOTTOM CONFIGURATION (LEWIS)  
10' x 10' SWT

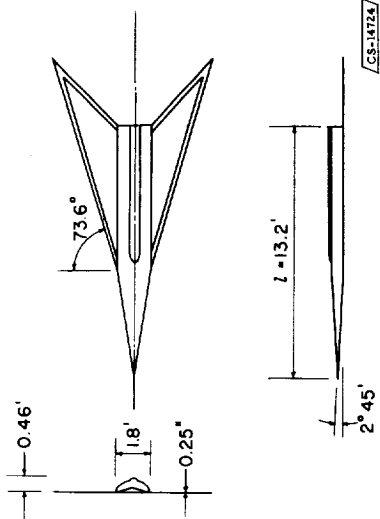


Figure 23(a)

CONVENTIONAL CONFIGURATION  
LEWIS 10' x 10' SWT



Figure 24

FLAT BOTTOM CONFIGURATION  
LEWIS 10' x 10' SWT



Figure 23(b)

RADIATION EQUILIBRIUM WALL TEMPERATURES  
TURBULENT BOUNDARY LAYER 0.8 EMISSIVITY

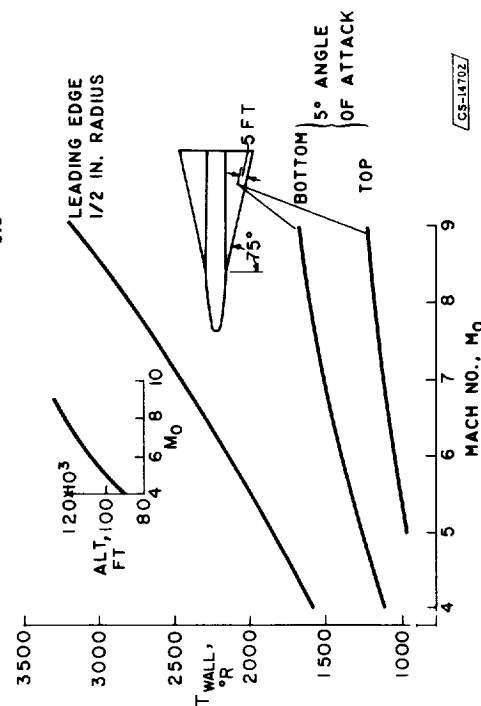


Figure 25

# ESTIMATED MINIMUM HYDROGEN TANK WEIGHTS

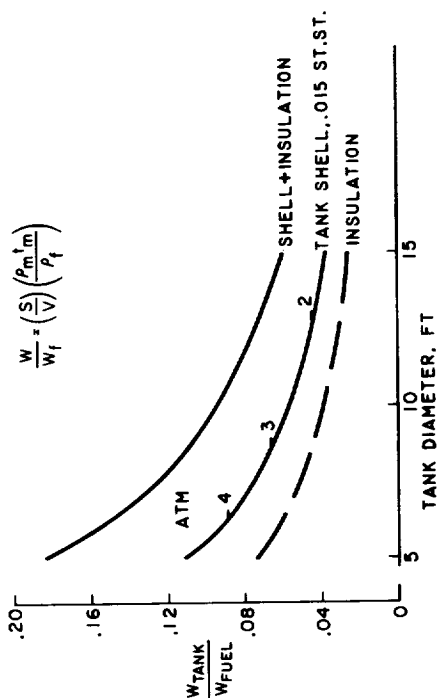


Figure 27

# HYDROGEN VAPORIZATION RATES

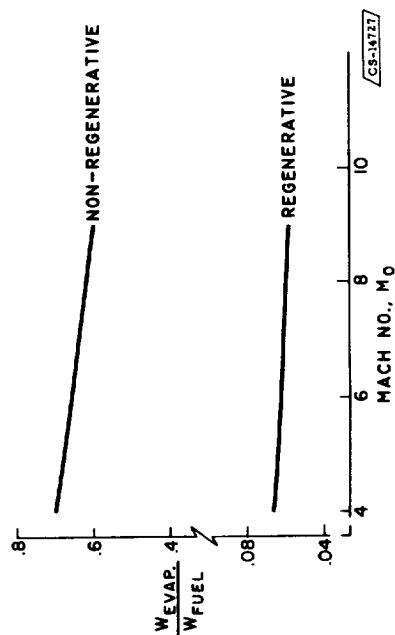


Figure 29

# AIRFRAME COOLING REQUIREMENT

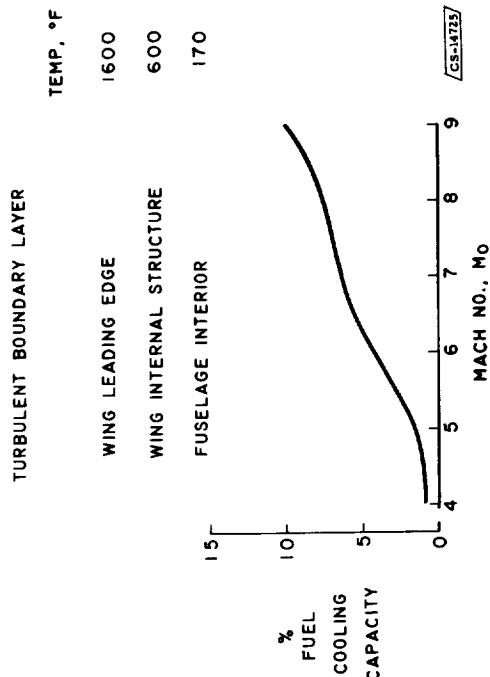


Figure 26

# HYDROGEN TANK INSULATION

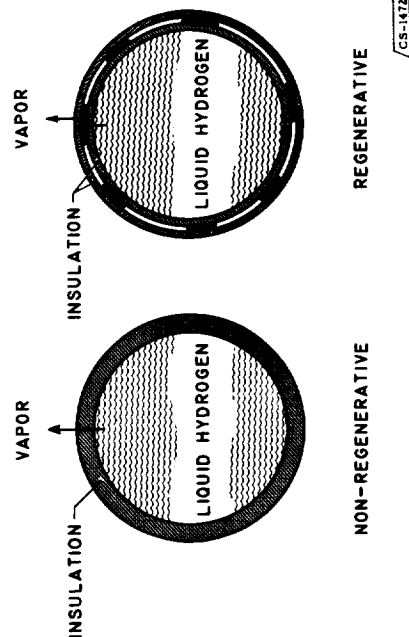


Figure 28

# IDEA AIRPLANE

FUEL, JP, GROSS WT, 500,000 LB, MACH NO. 4

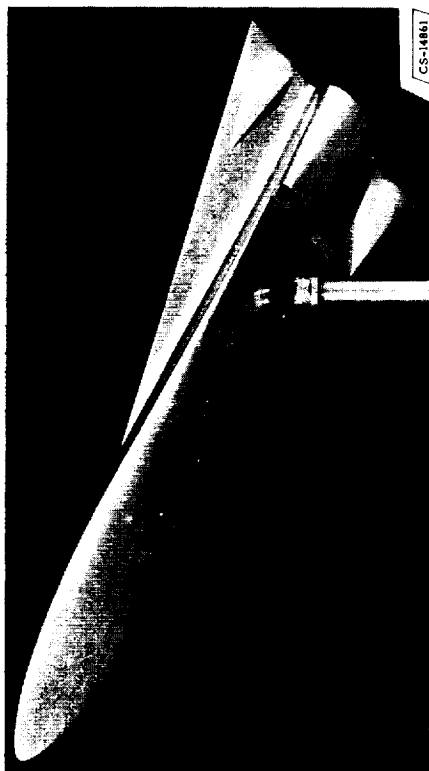


Figure 30(a)

# IDEA AIRPLANE

FUEL, HYDROGEN, GROSS WT, 300,000 LB, MACH NO. 4



Figure 30(b)

# IDEA ARROW WING AIRPLANE

FUEL, JP, GROSS WT, 500,000 LB, MACH NO. 3

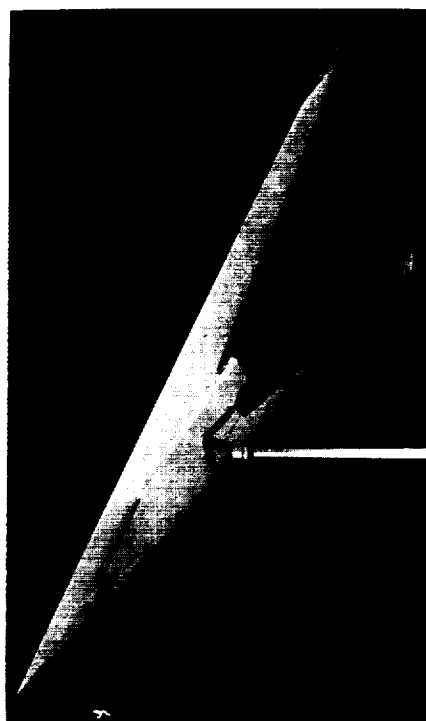


Figure 30(c)